I dedicate this thesis to my beloved parents (Maa and Papa), who have been my source of inspiration and my constant pillars of strength. I am forever grateful to them for all their sacrifices in making me what I am today.

To my wonderful family.....

Declaration

I hereby declare that the thesis entitled "Computational approaches to understand the interactions of small bioactive compounds and cell surface receptors with the SARS-CoV-2 viral proteins" has been submitted to Tezpur University in the Department of Molecular Biology and Biotechnology under the School of Sciences for partial fulfillment for the award of the degree of Doctor of Philosophy in Molecular Biology and Biotechnology.

I am the sole author of this thesis. This is a true copy of an original work carried out by me including any required final revisions, as accepted by my examiners.

Further, I declare that no part of this work has been reproduced elsewhere for award of any other degree.

Date: 23 | 07 | 2025

Place: Tezpur University, Tezpur

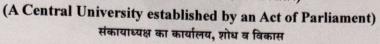
Chainee Das

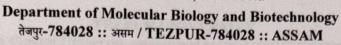
Chainee Das

Registration No.: TZ167371 of 2016

तेजपुर विश्वविद्यालय/TEZPUR UNIVERSITY

(संसद के अधिनियम द्वारा स्थापित केंद्रीय विश्वविद्यालय)







Dr. Venkata Satish Kumar Mattaparthi, M.Tech., Ph.D., Assistant Professor, of Molecular Biology and Biotechnology E-mail: venkata@tezu.ernet.in, mvenkatasatishkumar@gmail.com

Phone no: 918811806866/03712-275443

Fax: 03712-267005/267006(O)

CERTIFICATE OF THE PRINCIPAL SUPERVISOR

This is to certify that the thesis entitled "Computational approaches to understand the interactions of small bioactive compounds and cell surface receptors with the SARS-CoV-2 viral proteins" submitted to the School of Sciences, Tezpur University in partial fulfillment for the award of the degree of Doctor of Philosophy in Molecular Biology and Biotechnology is a record of original research work carried out by Miss Chainee Das under my personal supervision and guidance.

All helps received by her from various sources have been duly acknowledged. No part of this thesis has been reproduced elsewhere for award of any other degree.

Date: 23/07/2025

Place: Tezpur University, Tezpur

(Venkata Satish Kumar Mattaparthi)

Mole

Supervisor

Acknowledgements

First and foremost, I bow down my head to the almighty God for good health, wellbeing and for blessing me with immense patience that was necessary to complete this journey of Ph.D. successfully.

I would not have been able to complete this degree without the support of numerous people, for which I would like to acknowledge their support. First, I would like to express my sincerest gratitude towards my supervisor Dr. Venkata Satish Kumar Mattaparthi, for giving me this opportunity to work under his supervision and giving me freedom in my research and for his consistent encouragement that I have received throughout the research work. Under his guidance, I successfully overcame many difficulties and learned a lot. He always kept faith in me and guided me through the right direction whenever I needed it the most. My deep gratitude goes to him for all his dedication and steadiness during the writing of the thesis. I whole-heartedly thank him for everything.

I would also like to thank Prof. Rupak Mukhopadhyay, the Head of the Department of MBBT, Tezpur University, Prof. Robin Doley, Former Head, Department of MBBT, and my Doctoral Committee members — Prof. M. Mandal and Dr. S. Dasgupta, Department of MBBT, Tezpur University, for their insight, comments, and valuable suggestions during my Ph.D. tenure.

I would like to acknowledge all other faculty members in the Department of MBBT, Tezpur University for their help and

encouragement and the non-teaching staffs of the Department for their technical support. I would like to take this opportunity to thank Tezpur University for providing me with the state-of-the-art infrastructure and facilities for advanced research.

I would like to acknowledge the financial support provided by Tezpur University.

No word would be enough for expressing my gratitude towards lab seniors and juniors in MOMO Lab: Pundarikaksha daa, Priyanka baa, Dorothy baa, Babli, Prerana, Trishna, Khyati and Himanshu for their immense help and support. Heartfelt thanks to all the project students of our lab during my PhD tenure for their help and support.

I would like to express my gratitude to my batchmates for supporting me in many occasions during this work and for all the time we spent together.

Above ground, my biggest thanks goes to my father, my mother, my brother and my partner Prabin Daa for their fulltime support, motivation and unconditional love and for giving me a meaningful life. Love you all.

Regards, Chainee Das

Figure No.	Chapter 1	Page No.
1.1.	Depicts the (A) structural elements of the virus, including the spike protein, envelope, membrane, and nucleocapsid proteins along with (B) the SARS-CoV-2 genome components	2
Figure No.	Chapter 2	Page No.
2.1.	A three-dimensional (3-D) structure of the novel coronavirus (COVID-19).	11
2.2.	(A) The structural elements of the virus, including the spike protein, envelope, membrane, and internal components such as the viral single-stranded RNA and nucleocapsid proteins (B) SARS-CoV-2 genome components	12
2.3.	Viral life cycle of SARS-CoV-2.	13
2.4.	Schematic diagram of the transmission process of three HCoVs. Humans acquired SARS-CoV and MERS-CoV from bats through civet cats and dromedary camels, respectively. It is unclear how SARS-CoV-2 spread to humans	15
2.5.	Timeline for the emergence of human coronaviruses.	16
2.6.	The common, uncommon, and severe symptoms in patients with COVID-19.	17
2.7.	Schematic representation of SARS-CoV-2 Transmission Routes	19
2.8.	Showing the body systems and organs affected during COVID-19	23
2.9.	Showing the COVID-19 major events in India.	25
2.10.	Timeline of SARS-CoV-2 variant emergence	30
2.11.	SARS-CoV-2 virus depicting the location of the nucleocapsid (N), membrane (M), envelope (E), and spike (S) protein and zooming out the S protein	33
2.12.	Schematic representation of the SARS-CoV-2 spike protein organization.	34
2.13.	Angiotensin-converting enzyme 2 (ACE2) expression throughout the body. The organs vulnerability to SARS-CoV-2 infection is also indicated (high susceptibility).	36
2.14.	Surface representation of the spike, with monomers coloured in blue, rosy brown and gold, and ACE2 coloured in green.	37

2.15.	(A) The 3D structure of severe acute respiratory syndrome coronavirus	40
	2 (SARS-CoV-2) 3CLpro (pale green, PDB: 6XHU) and severe acute	
	respiratory syndrome coronavirus (SARS-CoV) 3CLpro (slate, PDB:	
	1UJ1). (B) Three structural domains (domain I: orange, domain II:	
	yellow, domain III: blue) of SARS-CoV-2 3CLpro monomer	
2.16.	Domain organization of the monomeric structure of the SARS-CoV-2	41
	3CLpro.	
		I
Figure	Chapter 3	Page
No.		No.
3.1.	Schematic illustration of the main contribution to the notantial energy	86
J.1.	Schematic illustration of the main contribution to the potential energy function.	80
3.2.	Periodic boundary conditions in two dimensions. The simulation cell	89
	(dark color) is surrounded by translated copies of itself (light color).	
3.3.	Schematic flowchart of steps involved in MD Simulation.	90
3.4.	Schematic representation of TIP3P water model.	92
3.5.	A schematic representation of the Different phases of a molecule	93
	during minimization of its energy.	
3.6.	Comparison of three optimization methods—(a) Steepest Descent, (b)	94
	Newton's Method, and (c) Conjugate Gradient—on a quadratic	
	function.	
3.7.	A line search is used to locate the minimum in the function in the	94
	direction of the gradient.	
3.8.	Working principle of Umbrella Sampling.	100
3.9.	The PatchDock user interface: The receptor molecule and the ligand	103
	molecule are given either by the PDB code of the molecule (chain IDs	
	are optional) or by uploading a file in PDB format.	
3.10.	Representation of the ClusPro algorithm, the number of structures	104
	retained after each step is shown in a blue box.	
3.11.	The Haddock user interface: (A) Entries required for the molecule 1	105
	and (B) Entries required for the molecule 2.	
3.12.	Computational schemes of the binding free energies based on MM-	107
	PBSA/GBSA.	
3.13.	Example output of PRODIGY showing the (A)input and (B) output	111
	page	
3.14.	Example output of HawkDock for the Spike-ACE2 complex	111

		1
3.15.	Protein–protein interaction diagrams in PDBsum (A) A schematic diagram showing the numbers of interactions across one of the interfaces, namely the A–B protein interface, and the numbers of residues involved in the Spike (Delta-plus)-ACE2 complex. (B) Detail	113
	of the individual residue–residue interactions across this interface.	
3.16.	LigPlot analysis showing hydrophobic interaction, hydrogen bonds between Main Protease and Rosmanol molecule	114
3.17.	Showing the main steps of Mapiya server to analyze the biomolecular interactions of proteins and their complexes (protein-protein, and protein with RNA and/or DNA).	115
3.18.	The primary CASTp server user interface. (A) The panel in the pocket and (B) sequence panels	117
Figure No.	Chapter 4	Page No.
4.1.	SARS-CoV-2 main protease (2019-nCoV, coronavirus disease 2019, COVID-19)	135
4.2.	Pictorial representation of the secondary structure predicted using GOR IV for Mpro	138
4.3.	Showing the alignments of the SARS-CoV and SARS-CoV-2 Mpro sequences aligned using Clustal Omega	138
4.4.	Intrinsically disordered prediction for Mpro using PONDR® VLXT	139
4.5.	3D structure of the entire SARS-CoV-2 Spike protein along with the	140
	Receptor binding domain (RBD) highlighted in green.	
4.6.	Cartoon representations of the down (left), Intermediate (middle) and up (right) state SARS-CoV-2 structures (PDB 6VXX, 7W94 and 6VYB, respectively)	141
4.7.	Pictorial representation of the secondary structure predicted using GOR IV for the RBD of the spike	144
4.8.	Pictorial representation of the secondary structure predicted using GOR IV for the entire spike.	144
4.9.	Showing the alignments of the SARS-CoV and SARS-CoV-2 RBD sequences aligned using Clustal Omega	145
4.10.	Showing the % identity of several variants of SARS-CoV-2 compared to the wild type.	145
4.11.	Intrinsically disordered prediction for the RBD of spike using PONDR® VLXT	146
4.12.	Intrinsically disordered prediction for the entire spike protein using PONDR® VLXT	146
4.13.	The pictorial representation of the summarized intermolecular interactions between S protein and ACE2 in (A) S protein (closed)-ACE2 complex (B) S protein (Intermediate)-ACE2 complex and (C) S protein (Open)-ACE2 complex	148

Figure No.	Chapter 5	Page No.
5.1.	Flowchart representing the methods and protocols followed in this work	163
5.2.	(A) Density, (B) Temperature, and (C) Energy plots of SARS-CoV-2-Alpha-ketomaide complex system as a function of simulation time.	164
5.3.	(A) Density, (B) Temperature, and (C) Energy plots of SARS-CoV-2-Arjunglucoside-I complex system as a function of simulation time.	165
5.4.	(A) Density, (B) Temperature, and (C) Energy plots of SARS-CoV-2-Carnosol complex system as a function of simulation time.	165
5.5.	(A) Density, (B) Temperature, and (C) Energy plots of SARS-CoV-2-Rosmanol complex system as a function of simulation time.	166
5.6.	Potential of Mean Force for the association and dissociation of the SARS-CoV-2 Mpro-small molecule complexes	167
5.7.	Convergence of the PMFs calculated by umbrella sampling for (A) SARS-CoV-2-Alpha-ketoamide (B) SARS-CoV-2-Arjunglucoside-I (C) SARS-CoV-2-Carnosol (D) SARS-CoV-2-Rosmanol complex where 5 ns US simulation were performed.	167
5.8.	Snapshots of SARS-CoV-2 (A)Mpro-Alpha-ketoamide complex structures, (B) Mpro-Arjunglucoside-I complex, (C) Mpro-Carnosol complex structures and (D) Mpro-Rosmanol complex structures at discrete distance of separation (in Å) between their centre of mass.	169
5.9.	Root Mean Square Deviation (RMSD) analysis of the SARS-CoV-2 Mpro-small molecule inhibitor complexes as a function of simulation time in picoseconds (ps).	172
5.10.	Root Mean Square Deviation (RMSD) analysis of the small molecule inhibitors in the complexes as a function of simulation time in picoseconds (ps).	172
5.11.	Root Mean Square Fluctuation (RMSF) Analysis of the SARS-CoV-2 Mpro-small molecule inhibitor complexes as a function of Residue index.	173
5.12.	Radius of gyration analysis (Rg) of the SARS-CoV-2 Mpro-small molecule inhibitor complexes as a function of simulation time in picoseconds (ps).	174
5.13.	Amino acid residual interactions of the protein-ligand interface in (A) SARS-CoV-2-Alpha-ketoamide (B) SARS-CoV-2-Arjunglucoside-I (C) SARS-CoV-2-Carnosol (D) SARS-CoV-2-Rosmanol complexes.	182

5.14.	Number of inter-molecular hydrogen bonds between SARS-CoV-2	183
	Mpro and the small molecule inhibitors as a function of simulation time	
	in picoseconds (ps).	
5.15.	Decomposition of the binding free energy on (A) per-residue basis (B)	190
	per-residue basis into contribution from vdW energy, the sum of	
	electrostatic energy and polar solvation energy and non-polar solvation	
	energy for SARS-CoV-2 Mpro-Alpha ketoamide complex.	
5.16.	Decomposition of the binding free energy on (A) per-residue basis (B)	191
0.10.	per-residue basis into contribution from vdW energy, the sum of	171
	electrostatic energy and polar solvation energy and non-polar solvation	
	energy for SARS-CoV-2 Mpro-Arjunglucoside –I complex	
5.17.	Decomposition of the binding free energy on (A) per-residue basis (B)	192
3.17.	per-residue basis into contribution from vdW energy, the sum of	172
	electrostatic energy and polar solvation energy and non-polar solvation	
	energy for SARS-CoV-2 Mpro-Carnosol complex	
5.18.	Decomposition of the binding free energy on (A) per-residue basis (B)	193
3.10.	per-residue basis into contribution from vdW energy, the sum of	173
	electrostatic energy and polar solvation energy and non-polar solvation	
	energy for SARS-CoV-2 Mpro-Rosmanol complex	
	energy for SAKS-Cov-2 Mpro-Rosmanor complex	
Hionre	Chapter 6	Page
Figure No.	Chapter 6	Page No.
No.	Chapter 6	Page No.
•		_
No.	The 3-D structure of SARS-CoV-2 Main protease (Mpro) bound with	No.
No. 6.1.	The 3-D structure of SARS-CoV-2 Main protease (Mpro) bound with Histone deacetylase 2 (HDAC2).	No. 205
No.	The 3-D structure of SARS-CoV-2 Main protease (Mpro) bound with	No.
6.1. 6.2.	The 3-D structure of SARS-CoV-2 Main protease (Mpro) bound with Histone deacetylase 2 (HDAC2). Superimposition of the Mpro-HDAC2 complex obtained from Cluspro and HDOCK.	205 206
No. 6.1.	The 3-D structure of SARS-CoV-2 Main protease (Mpro) bound with Histone deacetylase 2 (HDAC2). Superimposition of the Mpro-HDAC2 complex obtained from Cluspro and HDOCK. Ramachandran plot obtained from PROCHECK for the validation of	No. 205
6.1. 6.2. 6.3.	The 3-D structure of SARS-CoV-2 Main protease (Mpro) bound with Histone deacetylase 2 (HDAC2). Superimposition of the Mpro-HDAC2 complex obtained from Cluspro and HDOCK. Ramachandran plot obtained from PROCHECK for the validation of the Mpro-HDAC2 complex structure	205 206 206
No. 6.1. 6.2. 6.3.	The 3-D structure of SARS-CoV-2 Main protease (Mpro) bound with Histone deacetylase 2 (HDAC2). Superimposition of the Mpro-HDAC2 complex obtained from Cluspro and HDOCK. Ramachandran plot obtained from PROCHECK for the validation of the Mpro-HDAC2 complex structure Designing of the peptides from the parent sequence.	205 206 206 208
6.1. 6.2. 6.3.	The 3-D structure of SARS-CoV-2 Main protease (Mpro) bound with Histone deacetylase 2 (HDAC2). Superimposition of the Mpro-HDAC2 complex obtained from Cluspro and HDOCK. Ramachandran plot obtained from PROCHECK for the validation of the Mpro-HDAC2 complex structure Designing of the peptides from the parent sequence. The docked complexes for all the 13 peptides (shown in different	205 206 206
No. 6.1. 6.2. 6.3. 6.4. 6.5.	The 3-D structure of SARS-CoV-2 Main protease (Mpro) bound with Histone deacetylase 2 (HDAC2). Superimposition of the Mpro-HDAC2 complex obtained from Cluspro and HDOCK. Ramachandran plot obtained from PROCHECK for the validation of the Mpro-HDAC2 complex structure Designing of the peptides from the parent sequence. The docked complexes for all the 13 peptides (shown in different colors) and Mpro (purple)	205 206 206 208 210
No. 6.1. 6.2. 6.3.	The 3-D structure of SARS-CoV-2 Main protease (Mpro) bound with Histone deacetylase 2 (HDAC2). Superimposition of the Mpro-HDAC2 complex obtained from Cluspro and HDOCK. Ramachandran plot obtained from PROCHECK for the validation of the Mpro-HDAC2 complex structure Designing of the peptides from the parent sequence. The docked complexes for all the 13 peptides (shown in different colors) and Mpro (purple) Snapshots of SARS-CoV-2 Mpro apoprotein structures at discrete time	205 206 206 208
6.1. 6.2. 6.3. 6.4. 6.5.	The 3-D structure of SARS-CoV-2 Main protease (Mpro) bound with Histone deacetylase 2 (HDAC2). Superimposition of the Mpro-HDAC2 complex obtained from Cluspro and HDOCK. Ramachandran plot obtained from PROCHECK for the validation of the Mpro-HDAC2 complex structure Designing of the peptides from the parent sequence. The docked complexes for all the 13 peptides (shown in different colors) and Mpro (purple) Snapshots of SARS-CoV-2 Mpro apoprotein structures at discrete time interval during the 200 ns MD simulation	205 206 206 208 210 226
No. 6.1. 6.2. 6.3. 6.4. 6.5.	The 3-D structure of SARS-CoV-2 Main protease (Mpro) bound with Histone deacetylase 2 (HDAC2). Superimposition of the Mpro-HDAC2 complex obtained from Cluspro and HDOCK. Ramachandran plot obtained from PROCHECK for the validation of the Mpro-HDAC2 complex structure Designing of the peptides from the parent sequence. The docked complexes for all the 13 peptides (shown in different colors) and Mpro (purple) Snapshots of SARS-CoV-2 Mpro apoprotein structures at discrete time interval during the 200 ns MD simulation Snapshots of SARS-CoV-2 Mpro-peptide2 complex structures at	205 206 206 208 210
No. 6.1. 6.2. 6.3. 6.4. 6.5. 6.6.	The 3-D structure of SARS-CoV-2 Main protease (Mpro) bound with Histone deacetylase 2 (HDAC2). Superimposition of the Mpro-HDAC2 complex obtained from Cluspro and HDOCK. Ramachandran plot obtained from PROCHECK for the validation of the Mpro-HDAC2 complex structure Designing of the peptides from the parent sequence. The docked complexes for all the 13 peptides (shown in different colors) and Mpro (purple) Snapshots of SARS-CoV-2 Mpro apoprotein structures at discrete time interval during the 200 ns MD simulation Snapshots of SARS-CoV-2 Mpro-peptide2 complex structures at discrete time interval during the 200 ns MD simulation.	205 206 206 208 210 226 227
6.1. 6.2. 6.3. 6.4. 6.5.	The 3-D structure of SARS-CoV-2 Main protease (Mpro) bound with Histone deacetylase 2 (HDAC2). Superimposition of the Mpro-HDAC2 complex obtained from Cluspro and HDOCK. Ramachandran plot obtained from PROCHECK for the validation of the Mpro-HDAC2 complex structure Designing of the peptides from the parent sequence. The docked complexes for all the 13 peptides (shown in different colors) and Mpro (purple) Snapshots of SARS-CoV-2 Mpro apoprotein structures at discrete time interval during the 200 ns MD simulation Snapshots of SARS-CoV-2 Mpro-peptide2 complex structures at discrete time interval during the 200 ns MD simulation. Snapshots of SARS-CoV-2 Mpro-peptide4 complex structures at	205 206 206 208 210 226
No. 6.1. 6.2. 6.3. 6.4. 6.5. 6.6. 6.7.	The 3-D structure of SARS-CoV-2 Main protease (Mpro) bound with Histone deacetylase 2 (HDAC2). Superimposition of the Mpro-HDAC2 complex obtained from Cluspro and HDOCK. Ramachandran plot obtained from PROCHECK for the validation of the Mpro-HDAC2 complex structure Designing of the peptides from the parent sequence. The docked complexes for all the 13 peptides (shown in different colors) and Mpro (purple) Snapshots of SARS-CoV-2 Mpro apoprotein structures at discrete time interval during the 200 ns MD simulation Snapshots of SARS-CoV-2 Mpro-peptide2 complex structures at discrete time interval during the 200 ns MD simulation. Snapshots of SARS-CoV-2 Mpro-peptide4 complex structures at discrete time interval during the 200 ns MD simulation.	205 206 206 208 210 226 227 228
No. 6.1. 6.2. 6.3. 6.4. 6.5. 6.6.	The 3-D structure of SARS-CoV-2 Main protease (Mpro) bound with Histone deacetylase 2 (HDAC2). Superimposition of the Mpro-HDAC2 complex obtained from Cluspro and HDOCK. Ramachandran plot obtained from PROCHECK for the validation of the Mpro-HDAC2 complex structure Designing of the peptides from the parent sequence. The docked complexes for all the 13 peptides (shown in different colors) and Mpro (purple) Snapshots of SARS-CoV-2 Mpro apoprotein structures at discrete time interval during the 200 ns MD simulation Snapshots of SARS-CoV-2 Mpro-peptide2 complex structures at discrete time interval during the 200 ns MD simulation. Snapshots of SARS-CoV-2 Mpro-peptide4 complex structures at	205 206 206 208 210 226 227

6.10.	Backbone RMSD's for Mpro Apoprotein (violet), Mpro in Mpro-	230
	peptide4 complex (green) and Mpro in Mpro-peptide2 complex (red)	
6.11.	Backbone RMSF's for Mpro in Apoprotein (purple), Mpro-peptide4 complex (green) and Mpro-peptide2 complex (red).	231
6.12.	The number of intermolecular hydrogen bonds between (A) Mpro-	232
	peptide2 complex (Red-black) and (B) Mpro-peptide4 complex (Green-black)	
6.13.	Decomposition of binding free energy (kcal/mol) on per residue basis for Mpro binding to peptide2 obtained using MM-GBSA approach for (A) Mpro (violet) and (B) peptide2 (Red)	239
6.14.	Decomposition of binding free energy (kcal/mol) on per residue basis for Mpro binding to peptide4 obtained using MM-GBSA approach for (A) Mpro (violet) (B) peptide4 (green)	239
Figure	Chapter 7	Page
No.		No.
7.1	The discount of (A) CARC CAY 2 will are the	251
7.1.	Three-dimensional structure of (A) SARS-CoV-2 spike receptor-binding domain bound with ACE2 (PDB ID: 6lzg) (S protein (WT)-	251
	ACE2) (B) double mutant (L452R and E484Q) of SARS-CoV-2 spike	
	receptor-binding domain bound with ACE2 (S protein (DM)-ACE2).	
7.2.	Conformational snapshots of S protein (WT)-ACE2 complex at the	255
,,_,	time interval of 10 ns during the course of 100 ns MD simulation	200
7.3.	Conformational snapshots of S protein (DM)-ACE2 complex at the	256
	time interval of 10 ns during the course of 100 ns of MD simulation	
7.4.	Backbone RMSD's for (A) S protein (WT) apo (black), S protein (WT)-ACE2 complex (red) (B) S protein (DM) apo (black), S protein (DM)-ACE2 complex (red).	257
7.5.	RMSD plot of the residue at position (A) 452 (B) 484 in the S protein (WT)-ACE2 complex (black) and S protein (DM)-ACE2 complex (red).	258
7.6.	Backbone RMSF's for S protein in (A) S protein (WT)-ACE2 complex (black) (B) S protein (DM)-ACE2 complex (red).	258
7.7.	Number of intermolecular hydrogen bonds between S protein and	259
	ACE2 in (A) S protein (WT)-ACE2 complex (B) S protein (DM)-	
	ACE2 complex.	
7.8.	Intermolecular interactions at residue level between ACE2 and S protein in (A) S protein (WT)-ACE2 and (B) S protein (DM)-ACE2 complexes.	260

7.9.	Decemberation of hinding free energy (Iraal/mal) on non-regidue hasis	271
7.9.	Decomposition of binding free energy (kcal/mol) on per residue basis	2/1
	for ACE2 binding to S protein (WT) obtained using (A) MM-GBSA	
7.10	approach (B) MM-PBSA approach.	272
7.10.	Decomposition of binding free energy (kcal/mol) on per residue basis	272
	for ACE2 binding to S protein (DM) obtained using (A) MM-GBSA	
	approach (B) MM-PBSA approach.	
T.		D
Figure	Chapter 8	Page
No.		No.
8.1.	Three dimensional structure of (A) SARS CoV 2 spiles recentor	201
0.1.	Three-dimensional structure of (A) SARS-CoV-2 spike receptor-	281
	binding domain Delta variant bound with ACE2 (S protein (Delta)-	
	ACE2) (B) SARS-CoV-2 spike receptor-binding domain Delta Plus	
0.2	variant bound with ACE2 (S protein (Delta Plus)-ACE2)	204
8.2.	Snapshots of SARS-CoV-2 ACE2-Spike Protein (Delta variant)	284
	structures at discrete distance of separation (in Å) between their centre	
0.2	of mass.	20.4
8.3.	Snapshots of SARS-CoV-2 ACE2-Spike Protein (Delta-plus variant)	284
	structures at discrete distance of separation (in Å) between their centre	
0.4	of mass.	20.5
8.4.	Backbone RMSD's for (A) S protein (Delta) Apo (black), S protein	285
	(Delta)-ACE2 complex (red) (B) S protein (Delta-Plus) Apo (black), S	
0.=	protein (Delta-Plus)-ACE2 complex (red).	• • • •
8.5.	RMSD plot of the residue at position (A) 452 (B) 478 in S protein	286
	(WILD)-ACE2 complex (black), S protein (Delta)-ACE2 complex	
	(red) and S protein (Delta-Plus)-ACE2 complex (green)	• • • •
8.6.	RMSD plot of the residue at position 417 in S protein (WILD)-ACE2	286
	complex (black) and S protein (Delta-Plus)-ACE2 complex (green)	
8.7.	Backbone RMSF's for S protein in (A) S protein (WILD)-ACE2	287
	complex (black) (B) S protein (Delta)-ACE2 complex (red) and (C) S	
	protein (Delta-Plus)-ACE2 complex (green)	
8.8.	Number of intermolecular hydrogen bonds between S protein and	288
	ACE2 in (A) S protein (Delta)-ACE2 complex (B) S protein (Delta-	
	Plus)-ACE2 complex	
8.9.	Intermolecular interactions at residue level between ACE2 and S	303
	protein in (A) S protein (Delta)-ACE2 and (B) S protein (Delta-Plus)-	
	ACE2 complexes	
8.10.	Decomposition of binding free energy (kcal/mol) on per residue basis	305
	for ACE2 binding to S protein (Delta) obtained using (A) MM-GBSA	
	approach (B) MM-PBSA approach	

8.11.	Decomposition of binding free energy (kcal/mol) on per residue basis for ACE2 binding to S protein (Delta-Plus) obtained using (A) MM-GBSA approach (B) MM-PBSA approach	306
Figure No.	Chapter 9	Page No.
9.1.	3D structure of (A) SARS-CoV-2 spike receptor-binding domain of BA.1 variant bound with ACE2 (S protein (BA.1)-ACE2) (B) SARS-CoV-2 spike receptor-binding domain of BA.2 variant bound with ACE2 (S protein (BA.2)-ACE2).	316
9.2.	Snapshots of SARS-CoV-2 ACE2-Spike Protein (BA.1 variant) structures at discrete distance of separation (in Å) between their centre of mass.	318
9.3.	Snapshots of SARS-CoV-2 ACE2-Spike Protein (BA.2 variant) structures at discrete distance of separation (in Å) between their centre of mass.	319
9.4.	Backbone RMSD's for S protein (BA.1) Apo (black) and S protein (BA.1)-ACE2 complex (red)	321
9. 5.	Backbone RMSD's for S protein (BA.2) Apo (black) and S protein (BA.2)-ACE2 complex (red)	321
9.6.	RMSD plot of the common mutated residues at position (A) 339 (B) 373 (C) 375 (D) 417 (E) 440 (F) 477 (G) 478 (H) 484 (I) 493 (J) 498 (K) 501 (L) 505 in S protein (WILD)-ACE2 complex (black), S protein (BA.1)-ACE2 complex (red) and S protein (BA.2)-ACE2 complex (green)	322
9.7.	RMSD plot of the residues exclusively present in BA.1 at position (A) 371 (B) 446 (C) 496 in S protein (WILD)-ACE2 complex (black), S protein (BA.1)-ACE2 complex (red).	323
9.8.	RMSD plot of the residues exclusively present in BA.2 at position (A) 371 (B) 376 (C) 405 (D) 408 in S protein (WILD)-ACE2 complex (black), S protein (BA.2)-ACE2 complex (green).	323
9.9.	Backbone RMSF's for S protein in (A) S protein (WILD)-ACE2 complex (black) (B) S protein (BA.1)-ACE2 complex (red) and (C) S protein (BA.2)-ACE2 complex (green).	324
9.10.	Number of intermolecular hydrogen bonds between S protein and ACE2 in (A) S protein (BA.1)-ACE2 complex (B) S protein (BA.2)-ACE2 complex.	325
9.11.	Intermolecular interactions at residue level between ACE2 and S protein in (A) S protein (BA.1)-ACE2 and (B) S protein (BA.2)-ACE2 complex.	337

9.12.	Decomposition of binding free energy (kcal/mol) on per residue basis for (A) SPIKE (BA.1) and (B) ACE2 obtained using MM-GBSA approach	352
9.13.	Decomposition of binding free energy (kcal/mol) on per residue basis for (A) SPIKE (BA.2) and (B) ACE2 obtained using MM-GBSA approach	352
Figure	Chapter 10	Page
No.		No.
10.1.	3D structure of (A) SARS-CoV-2 spike receptor-binding domain of BA.4 variant bound with ACE2 (S protein (BA.4)-ACE2) (B) SARS-CoV-2 spike receptor-binding domain of BA.2.12.1 variant bound with ACE2 (S protein (BA.2.12.1)-ACE2).	363
10.2.	Representation of helix, sheet and coil regions of secondary structure of BA.2.12.1 variant predicted from GOR IV.	368
10.3.	Representation of helix, sheet and coil regions of secondary structure of BA.4 variant predicted from GOR IV.	368
10.4.	Clustal Omega was used to align the receptor binding region sequence ranging from 333-527 of the two variants- BA.2.12.1 and BA.4 with respect to BA.2.	369
10.5.	Conformational snapshots of S protein (BA.4)-ACE2 complex at the discrete time interval of 10 ns during the course of 100 ns of MD simulation.	370
10.6.	Conformational snapshots of S protein (BA.2.12.1)-ACE2 complex at the discrete time interval of 10 ns during the course of 100 ns of MD simulation.	371
10.7.	Backbone RMSD's for S protein (BA.4) Apo (black) and S protein (BA.4) in S protein (BA.4)-ACE2 complex (Red)	372
10.8.	Backbone RMSD's for S protein (BA.2.12.1) Apo (Red) and S protein (BA.2.12.1) in S protein (BA.2.12.1)-ACE2 complex (Black)	372
10.9.	Backbone RMSF's for Spike protein in (A) S protein (BA.4)-ACE2 complex (Green) and (B) S protein (BA.2.12.1)-ACE2 complex (Blue).	373
10.10.	Backbone RMSF's for (A) S protein (BA.4)-ACE2 complex (blue) and (B) S protein (BA.2.12.1)-ACE2 complex (red).	373
10.11.	Number of intermolecular hydrogen bonds between S protein and ACE2 in (A) S protein (BA.4)-ACE2 complex (B) S protein (BA.2.12.1)-ACE2 complex.	374
10.12.	Intermolecular interactions at residue level between ACE2 and S protein in (A) S protein (BA.4)-ACE2 and (B) S protein (BA.2.12.1) - ACE2 complex.	394

10.13.	Decomposition of binding free energy (kcal/mol) on per residue basis	207
10.13.	for (A) SPIKE (BA.4) and (B) ACE2 obtained using MM-GBSA approach	396
10.14.	Decomposition of binding free energy (kcal/mol) on per residue basis for (A) SPIKE (BA.2.12.1) and (B) ACE2 obtained using MM-GBSA	396
	approach	
T.		
Figure	Chapter 11	Page
No.		No.
11.1.	(A) BA.2.75 variant mutations in receptor-binding domain (RBD) of Spike protein. (B) BA.2.75 variant mutations in receptor-binding domain of spike protein bound with the ACE2 receptor. (C) BA.2.75.2 variant mutations in receptor-binding domain (RBD) of spike protein	406
	(D) BA.2.75.2 variant mutations in receptor-binding domain of spike protein bound with the ACE2 receptor.	
11.2.	PONDR score as a function of residue number analyzed for (A) BA.2.75 and (B) BA.2.75.2 using PONDR® VLXT	411
11.3.	Intrinsically disordered prediction for the complete sequence of spike protein of BA.2.75 variant showing the ordered regions represented by " " and disordered regions represented by "D", analyzed using PONDR® VLXT	413
11.4.	Intrinsically disordered prediction for the sequence of RBD of spike protein for BA.2.75 variant showing the ordered regions represented by " " and disordered regions represented by "D", analyzed using PONDR® VLXT	413
11.5.	Intrinsically disordered predictions for the sequence of complete spike protein for BA.2.75.2 variant showing the ordered regions represented by " " and disordered regions represented by "D", analyzed using PONDR® VLXT.	415
11.6.	Intrinsically disordered prediction for the sequence of RBD of spike protein for BA.2.75.2 variant showing the ordered regions represented by " " and disordered regions represented by "D", analyzed using PONDR® VLXT	416
11.7.	PONDR score as a function of residue number analyzed for the complete sequence of wild type Wuhan strain using PONDR® VLXT	417
11.8.	Intrinsically disordered prediction for the complete sequence of spike protein for wild type Wuhan-Hu-1 strain showing the ordered regions represented by " " and disordered regions represented by "D", analyzed using PONDR® VLXT	418
11.9.	Conformational snapshots of S protein (BA.2.75)-ACE2 complex at the time interval of 5 ns during the course of 100 ns of MD simulation.	432

	Conformational snapshots of S protein (BA.2.75.2)-ACE2 complex at the time interval of 5 ns during the course of 100 ns of MD simulation.	433
11.11.	Backbone RMSD's for S protein (BA.2.75)-ACE2 complex (black) and S protein (BA.2.75.2)-ACE2 complex (red).	434
11.12.	Backbone RMSD's for S protein in S protein (BA.2.75.2)-ACE2 complex (black) and S protein (BA.2.75)-ACE2 complex (red)	434
11.13.	Backbone RMSF's for S protein in S protein (BA.2.75)-ACE2 complex (black) and S protein (BA.2.75.2)-ACE2 complex (red).	435
11.14.	Backbone RMSF's for S protein (BA.2.75)-ACE2 complex (black) and S protein (BA.2.75.2)-ACE2 complex (red).	435
11.15.	The number of intermolecular hydrogen bonds between S protein and ACE2 in (A) S protein (BA.2.75)-ACE2 complex and (B) S protein (BA.2.75.2)-ACE2 complex	436
11.16.	Decomposition of binding free energy (kcal/mol) on per residue basis for ACE2 binding to S protein (BA.2.75) obtained using MM-GBSA approach for (A) Spike (BA.2.75) (B) ACE2.	441
11.17.	Decomposition of binding free energy (kcal/mol) on per residue basis for ACE2 binding to S protein (BA.2.75.2) obtained using MM-GBSA approach for (A) Spike (BA.2.75.2) (B) ACE2.	442
E	Chambar 10	Daga
Figure No.	Chapter 12	Page No.
12.1.	The 3-D structure of (A) SARS-CoV-2 spike receptor-binding domain bound with L-SIGN (S protein-L-SIGN) and (B) SARS-CoV-2 spike receptor-binding domain bound with CAT (S protein-CAT).	455
12.1.	bound with L-SIGN (S protein-L-SIGN) and (B) SARS-CoV-2 spike	455
	bound with L-SIGN (S protein-L-SIGN) and (B) SARS-CoV-2 spike receptor-binding domain bound with CAT (S protein-CAT). Conformational Snapshots of SARS-CoV-2 L-SIGN-Spike Protein	
12.2.	bound with L-SIGN (S protein-L-SIGN) and (B) SARS-CoV-2 spike receptor-binding domain bound with CAT (S protein-CAT). Conformational Snapshots of SARS-CoV-2 L-SIGN-Spike Protein structures at discrete interval of simulation time Conformational Snapshots of SARS-CoV-2 CAT-Spike Protein	456
12.2.	bound with L-SIGN (S protein-L-SIGN) and (B) SARS-CoV-2 spike receptor-binding domain bound with CAT (S protein-CAT). Conformational Snapshots of SARS-CoV-2 L-SIGN-Spike Protein structures at discrete interval of simulation time Conformational Snapshots of SARS-CoV-2 CAT-Spike Protein structures at discrete interval of simulation time. The RMSD of the backbone Cα atoms for (A) S protein-L-SIGN	456 457
12.2. 12.3. 12.4.	bound with L-SIGN (S protein-L-SIGN) and (B) SARS-CoV-2 spike receptor-binding domain bound with CAT (S protein-CAT). Conformational Snapshots of SARS-CoV-2 L-SIGN-Spike Protein structures at discrete interval of simulation time Conformational Snapshots of SARS-CoV-2 CAT-Spike Protein structures at discrete interval of simulation time. The RMSD of the backbone Cα atoms for (A) S protein-L-SIGN complex and (B) S protein-CAT complex The RMSF for the backbone Cα atoms (A) S protein (B) L-SIGN in S	456 457 458
12.2. 12.3. 12.4.	bound with L-SIGN (S protein-L-SIGN) and (B) SARS-CoV-2 spike receptor-binding domain bound with CAT (S protein-CAT). Conformational Snapshots of SARS-CoV-2 L-SIGN-Spike Protein structures at discrete interval of simulation time Conformational Snapshots of SARS-CoV-2 CAT-Spike Protein structures at discrete interval of simulation time. The RMSD of the backbone Cα atoms for (A) S protein-L-SIGN complex and (B) S protein-CAT complex The RMSF for the backbone Cα atoms (A) S protein (B) L-SIGN in S protein-L-SIGN complex. The RMSF for the backbone Cα atoms (A) S protein (B) CAT in S	456 457 458 459

12.9.	Decomposition of binding free energy (kcal/mol) on per residue basis for (A) SPIKE (B) L-SIGN receptor of the S protein-L-SIGN complex.	483
12.10.	Decomposition of binding free energy (kcal/mol) on per residue basis for (A) SPIKE (B) CAT receptor of the S protein-CAT complex.	484

Table	Chapter 4	
No.		No.
4.1	E-DACV D. AD 1-4- AM	136
4.1.	ExPASY ProtParam data of Mpro.	
4.2.	Secondary structure predicted using GOR IV for Mpro	137
4.3.	ExPASY ProtParam data of entire spike and RBD	143
4.4.	Secondary structure predicted using GOR IV for entire spike and RBD.	143
4.5.	Interface statistics for the S protein (Intermediate)-ACE2, S protein	147
	(Closed)-ACE2 and S protein (Open)-ACE2 complexes	1.10
4.6.	Binding free energy (ΔG) values between the S protein and ACE2 in	148
	the closed, intermediate and open state.	
- 11		_
Table	Chapter 5	Page
No.		No.
F 1	Details of the court of the last the court of the court o	157
5.1.	Details of the small molecule inhibitors obtained from Pubchem	157
<i>5</i> 2	database.	
5.2.	Details of Umbrella Sampling Simulation	
5.3.	List of atom-atom interactions(non-bonded) across protein-ligand	
- 4 4	interface in SARS-CoV2 Mpro- AKA complex from PDBsum server	
5.4A.	List of atom-atom interactions (Hydrogen bonds) across protein-	
	protein interface in SARS-Cov2- ARJ complex from PDBsum server.	175
5.4B.	List of atom-atom interactions (non-bonded) across protein-protein	
	interface in SARS-Cov2- ARJ complex from PDBsum server.	
5.5A.	List of atom-atom interactions (Hydrogen bonds) across protein-	177
	protein interface in SARS-Cov2- CAN complex from PDBsum server.	
5.5B.	List of atom-atom interactions (non-bonded) across protein-protein	177
	interface in SARS-Cov2- CAN complex from PDBsum server.	
5.6A.	List of atom-atom interactions across protein-protein interface in	180
	SARS-Cov2- ROS complex from PDBsum server.	
5.6B.	List of atom-atom interactions (non-bonded) across protein-protein	181
	interface in SARS-Cov2- ROS complex from PDBsum server.	
5.7.	The various components of the Binding Free Energy (kcal/mol)	184
	evaluated by Molecular Mechanics-Generalized Borne Surface Area	
	(MM-GBSA) method between SARS-CoV-2 main protease (Mpro) -	
	alpha ketoamide (AKA) complex.	

5.8.	The various components of the Binding Free Energy (kcal/mol) evaluated by Molecular Mechanics- Poisson-Boltzmann Surface Area	185
	(MM-PBSA) method between SARS-CoV-2 main protease (Mpro) –	
	alpha ketoamide (AKA) complex.	
5.9.	The various components of the Binding Free Energy (kcal/mol)	185
	evaluated by Molecular Mechanics-Generalized Borne Surface Area	
	(MM-GBSA) method between SARS-CoV-2 main protease (Mpro)-	
	arjunglucoside-I(ARJ) complex.	
5.10.	The various components of the Binding Free Energy (kcal/mol) evaluated by Molecular Mechanics-Poisson-Boltzmann Surface Area (MM-PBSA) method between SARS-CoV-2 main protease (Mpro)—Arjunglucoside-I (ARJ) complex.	186
5.11.	The various components of the Binding Free Energy (kcal/mol)	187
	evaluated by Molecular Mechanics-Generalized Borne Surface Area	
	(MM-GBSA) method between SARS-CoV-2 main protease (Mpro) –	
	Carsonol (CAN) complex.	
5.12.	The various components of the Binding Free Energy (kcal/mol)	187
	evaluated by Molecular Mechanics- Poisson-Boltzmann Surface Area	
	(MM-PBSA) method between SARS-CoV-2 main protease (Mpro) –	
	Carsonol (CAN complex).	
5.13.	The various components of the Binding Free Energy (kcal/mol)	188
	evaluated by Molecular Mechanics-Generalized Borne Surface Area (MM-GBSA) method between SARS-CoV-2 main protease (Mpro)-	
	Rosmanol (ROS) complex.	
5.14.	The various components of the Binding Free Energy (kcal/mol)	189
	evaluated by Molecular Mechanics-Poisson-Boltzmann Surface Area	
	(MM-PBSA) method between SARS-CoV-2 main protease (Mpro)-	
	Rosmanol (ROS) complex.	
Table	Chapter 6	Page
No.		No.
6.1.	Electrostatic contacts between Mpro and HDAC2 with distance less	207
	than or equal to 5 Å.	605
6.2.	Showing the sequences of all 13 designed peptides	208
6.3.	The toxicity analysis of all 13 peptides using ToxIBTL	211
6.4.	Binding free energy (ΔG) values between the Mpro and peptides.	211
6.5.	Binding free energy (ΔG) values between the Mpro and positive control	212
	peptides (3CVL-2, 3CVL-4, 3CVL-7)	615
6.6.A.	List of atom-atom interactions (Hydrogen bonds) across protein-	213
	peptide interface in Mpro (Chain A) and Peptide2 (Chain B) complex	
	from PDBsum server.	

6.6.B.	List of atom-atom interactions (non-bonded) across protein-peptide interface in Mpro (Chain A) and Peptide2 (Chain B) complex from PDBsum server	213
6.6. C.	List of atom-atom interactions (Salt Bridge) across protein-peptide interface in Mpro (Chain A) and Peptide2 (Chain B) complex from PDBsum server	217
6.7. A.	List of atom-atom interactions (Hydrogen bonds) across protein- peptide interface in Mpro (Chain A) and Peptide4 (Chain B) complex from PDBsum server	217
6.7.B.	List of atom-atom interactions (non-bonded) across protein-peptide interface in Mpro (Chain A) and Peptide4 (Chain B) complex from PDBsum server	218
6.7. C.	List of atom-atom interactions (Salt bridge) across protein-peptide interface in Mpro (Chain A) and Peptide4 (Chain B) complex from PDBsum server	221
6.8.	ADME analysis of peptide 2 and peptide 4 using ADMETLab2.0 tool	222
6.9.	Hydrogen bond analysis of Mpro-Peptide2 complex during the last 20 ns of MD simulation with Mpro as acceptor and peptide2 as donor.	232
6.10.	Hydrogen bond analysis of Mpro-Peptide2 complex during the last 20 ns of MD simulation with peptide2 as acceptor and Mpro as donor.	233
6.11.	Hydrogen bond analysis of Mpro-Peptide4 complex during the last 20 ns of MD simulation with Mpro as acceptor and peptide4 as donor.	235
6.12.	Hydrogen bond analysis of Mpro-Peptide4 complex during the last 20 ns of MD simulation with peptide4 as acceptor and Mpro as donor.	236
6.13.	Binding free energies (kcal/mol) and its components of Mpro-peptide2 complex obtained using MM-GBSA approach.	238
6.14.	Binding free energies (kcal/mol) and its components of Mpro-peptide4 complex obtained using MM-GBSA approach.	238
Table	Chapter 7	Page
No.		No.
7.1	I de Control C	260
7.1.	Interface statistics for the S protein (WT)-ACE2 and S protein(DM)-ACE2	260
7.2.	List of atom-atom interactions (Hydrogen bonds) across protein- protein interface in S protein (WT)–ACE2 complex from PDBsum server	261
7.3.	List of atom-atom interactions (non-bonded) across protein-protein interface in S protein (WT)–ACE2 complex from PDBsum server	262
7.4.	List of atom-atom interactions (salt bridges) across protein-protein interface in S protein (WT)–ACE2 complex from PDBsum server	264

7.5.	List of atom-atom interactions (Hydrogen bonds) across protein-	265
	protein interface in S protein (DM)-ACE2 complex from PDBsum	
	server	
7.6.	List of atom-atom interactions (non-bonded) across protein-protein	265
	interface in S protein (DM)–ACE2 complex from PDBsum server	
7.7.	List of atom-atom interactions (salt bridges) across protein-protein	270
	interface in S protein (DM)–ACE2 complex from PDBsum server	
7.8.	Binding free energies (kcal/mol) and its components of S protein (WT)-ACE2 and S protein (DM)-ACE2 complexes obtained using MM-GBSA approach.	270
7.9.	Binding free energies (kcal/mol) and its components of S protein (WT)-ACE2 and S protein (DM)-ACE2 complexes obtained using MM-PBSA approach	271
		_
Table	Chapter 8	Page
No.		No.
0.1	W. 1	200
8.1.	Hydrogen bond analysis of S protein (DELTA)-ACE2 complex during the last 20 ns of MD simulation with S protein as acceptor and ACE2 as donor	288
8.2.	Hydrogen bond analysis of S protein (DELTA)-ACE2 complex during	289
	the last 20 ns of MD simulation with S protein as donor and ACE2 as	
8.3.	acceptor Hydrogen bond analysis of S protein (DELTA PLUS)-ACE2 complex	290
0.5.	during the last 20 ns of MD simulation with S protein as acceptor and	270
	ACE2 as donor	
8.4.	Hydrogen bond analysis of S protein (DELTA PLUS)-ACE2 complex	291
	during the last 20 ns of MD simulation with S protein as donor and	
	ACE2 as acceptor.	
8.5.	Interface statistics for the S protein (Delta)-ACE2 and S protein (Delta-	292
	Plus)-ACE2 complexes.	
8.6.	List of atom-atom interactions (Hydrogen bonds) across protein-ligand	293
	interface in ACE2 (Chain A)-Spike Protein (Chain B) (Delta variant)	
	complex from PDBsum server	
8.7.	List of atom-atom interactions (Non-bonded contacts) across protein-	294
	ligand interface in ACE2 (Chain A)-Spike Protein (Chain B) (Delta	
	variant) complex from PDBsum server	
8.8.	List of atom-atom interactions (Salt bridge) across protein-ligand	297
	interface in ACE2 (Chain A)-Spike Protein (Chain B) (Delta variant)	
	complex from PDBsum server	
8.9.	List of atom-atom interactions (Hydrogen bonds) across protein-ligand	298
	interface in ACE2 (Chain A)-Spike Protein (Chain B) (Delta-Plus	
	variant) complex from PDBsum server	

8.10.	List of atom-atom interactions (Non-bonded contacts) across protein-	298
	ligand interface in ACE2 (Chain A)-Spike Protein (Chain B) (Delta- Plus variant) complex from PDBsum server	
8.11.	List of atom-atom interactions (Salt bridges) across protein-ligand interface in ACE2 (Chain A)-Spike Protein (Chain B) (Delta-Plus variant) complex from PDBsum server	302
8.12.	Binding free energies (kcal/mol) and its components of S protein (Delta)-ACE2 and S protein (Delta-Plus)-ACE2 complexes obtained using MM-GBSA approach	304
8.13.	Binding free energies (kcal/mol) and its components of S protein (Delta)-ACE2 and S protein (Delta-Plus)-ACE2 complexes obtained using MM-PBSA approach	304
Table	Chapter 9	Page
No.	Chapters	No.
9.1.	Showing mutations (in RBD of Spike Protein) of BA.1 and BA.2 lineages	317
9.2.	Hydrogen bond analysis of S protein (BA.1)-ACE2 complex during the last 20 ns of MD simulation with S protein as acceptor and ACE2 as donor.	325
9.3.	Hydrogen bond analysis of S protein (BA.1)-ACE2 complex during the last 20 ns of MD simulation with S protein as donor and ACE2 as acceptor.	327
9.4.	Hydrogen bond analysis of S protein (BA.2)-ACE2 complex during the last 20 ns of MD simulation with S protein as acceptor and ACE2 as donor.	330
9.5.	Hydrogen bond analysis of S protein (BA.2)-ACE2 complex during the last 20 ns of MD simulation with S protein as donor and ACE2 as acceptor.	332
9.6.	Interface statistics for the S protein (BA.1)-ACE2 and S protein (BA.2)-ACE2 complexes.	337
9.7.	List of atom-atom interactions (Hydrogen bonds) across protein-ligand interface in ACE2(chain A)-Spike Protein (Chain B) (BA.1variant) complex from PDBsum server	338
9.8.	List of atom-atom interactions (non-bonded contacts) across protein- ligand interface in ACE2(chain A)-Spike Protein (Chain B) (BA.1variant) complex from PDBsum server	339
9.9.	List of atom-atom interactions (Salt bridges) across protein-ligand interface in ACE2(chain A)-Spike Protein (Chain B) (BA.1variant) complex from PDBsum server	345

9.10.	List of atom-atom interactions (Hydrogen bonds) across protein-ligand interface in ACE2 (Chain A)-Spike Protein (Chain B) (BA.2 variant) complex from PDBsum server	345
9.11.	List of atom-atom interactions (non-bonded contacts) across protein-ligand interface in ACE2 (Chain A)-Spike Protein (Chain B) (BA.2 variant) complex from PDBsum server.	345
9.12.	List of atom-atom interactions (Salt bridges) across protein-ligand interface in ACE2 (Chain A)-Spike Protein (Chain B) (BA.2 variant) complex from PDBsum server.	350
9.13.	Binding free energies (kcal/mol) and its components of S protein (BA.1)-ACE2 and S protein (BA.2)-ACE2 complexes obtained using MM-GBSA approach	351
Table No.	Chapter 10	Page No.
10.1.	Mutations (in RBD of Spike Protein) of BA.4 and BA.2.12.1 lineages along with the common mutations on both the lineages.	363
10.2.	ExPASY ProtParam data of BA.2.12.1 and BA 4 variant.	366
10.3.	Structural changes in the RBD region of BA.2.12.1 and BA.4 predicted using GOR IV	367
10.4.	Intrinsically disordered prediction using PONDR® VLXT	369
10.5.	Hydrogen bond analysis of S protein (BA.4)-ACE2 complex during the	375
	last 20 ns of MD simulation with S protein as acceptor and ACE2 as	
	donor.	
10.6.	Hydrogen bond analysis of S protein (BA.4)-ACE2 complex during the last 20 ns of MD simulation with S protein as donor and ACE2 as acceptor.	376
10.7.	Hydrogen bond analysis of S protein (BA.2.12.1)-ACE2 complex during the last 20 ns of MD simulation with S protein as acceptor and ACE2 as donor.	378
10.8.	Hydrogen bond analysis of S protein (BA.2.12.1)-ACE2 complex during the last 20 ns of MD simulation with S protein as donor and ACE2 as acceptor.	380
10.9.	Interface statistics for the S protein (BA.4)-ACE2 and S protein (BA.2.12.1)-ACE2 complexes.	382
10.10.	List of atom-atom interactions (Salt bridges) across protein-ligand interface in Spike Protein (BA.2.12.1) (Chain A) and ACE2 receptor (Chain B) complex from PDBsum server	383
10.11.	List of atom-atom interactions (Hydrogen bonds) across protein-ligand interface in Spike Protein (BA.2.12.1) (Chain A) and ACE2 receptor (Chain B) complex from PDBsum server	383

10.12.	List of atom-atom interactions (non-bonded contacts) across protein-	
	ligand interface in Spike Protein (BA.2.12.1) (Chain A) and ACE2	
	receptor (Chain B) complex from PDBsum server	
10.13.	List of atom-atom interactions (Salt bridges) across protein-ligand	389
	interface in Spike Protein (BA.4) (Chain A) and ACE2 receptor (Chain	
	B) complex from PDBsum server	
10.14.	List of atom-atom interactions (Hydrogen bonds) across protein-ligand	389
	interface in Spike Protein (BA.4) (Chain A) and ACE2 receptor (Chain	
10.17	B) complex from PDBsum server	200
10.15.	List of atom-atom interactions (non-bonded contacts) across protein-	389
	ligand interface in Spike Protein (BA.4) (Chain A) and ACE2 receptor	
10.16	(Chain B) complex from PDBsum server	207
10.16.	Binding free energies (kcal/mol) and its components of S protein	395
	(BA.4)-ACE2 and S protein (BA.2.12.1.12.1)-ACE2 complexes	
	obtained using MM-GBSA approach.	
Table	Chapter 11	Daga
	Chapter 11	Page
No.		No.
44.4		100
11.1.	Spike protein mutation in BA.2.75 and BA.2.75.2 variant compared to	409
11.0	wild-type (Wuhan-Hu-1)	410
11.2.	Secondary structure analysis for BA.2.75 and BA.2.75.2 variant	410
11.3.	The Identity and similarity percentage in the amino acid sequence for	410
11.4	Wild type (WT) and Omicron variants (BA.2.75 and BA.2.75.2).	411
11.4.	Intrinsically disordered prediction for BA.2.75 variant using PONDR® VLXT	411
11.5.	Intrinsically disordered prediction for BA.2.75.2 variant using PONDR® VLXT	411
11.6.	Intrinsically disordered prediction for the complete sequence of wild	416
	type strain using PONDR® VLXT	
11.7.	I-mutant 3.0 analysis on the spike protein of the BA.2.75 and BA.2.75.2	419
	variant	
11.8.	Interface statistics for the S protein (BA.2.75)-ACE2 and S protein	420
	(BA.2.75.2)-ACE2 complexes	
11.9.	List of atom-atom interactions (Hydrogen bonds) across protein-ligand	421
	interface in ACE2 (chain A)-Spike Protein (Chain B) (BA.2.75 variant)	
	complex from PDBsum server	
11.10.	List of atom-atom interactions (non-bonded contacts) across protein-	421
	ligand interface in ACE2 (chain A)-Spike Protein (Chain B)	
	(BA.2.75variant) complex from PDBsum server	

11.11.	List of atom-atom interactions (Hydrogen bonds) across protein-ligand	425
	interface in ACE2 (chain A)-Spike Protein (Chain B) (BA.2.75.2	
	variant) complex from PDBsum server	
11.12.	List of atom-atom interactions (non-bonded contacts) across protein-	425
	ligand interface in ACE2 (chain A)-Spike Protein (Chain B) (BA.2.75.2	
	variant) complex from PDBsum server	
11.13.	SIFT analysis for BA.2.75 variant	429
11.14.	SIFT analysis for BA.2.75.2 variant	430
11.15.	Hydrogen bond analysis of S protein (BA.2.75)-ACE2 complex during	436
	the last 20 ns of MD simulation with S protein (BA.2.75) as acceptor	
	and ACE2 as donor.	
11.16.	Hydrogen bond analysis of S protein (BA.2.75)-ACE2 complex during	437
	the last 20 ns of MD simulation with S protein (BA.2.75) as donor and	
	ACE2 as acceptor	
11.17.	Hydrogen bond analysis of S protein (BA.2.75.2)-ACE2 complex	438
	during the last 20 ns of MD simulation with S protein (BA.2.75.2) as	
	acceptor and ACE2 as donor.	
11.18.	Hydrogen bond analysis of S protein (BA.2.75.2)-ACE2 complex	439
	during the last 20 ns of MD simulation with S protein (BA.2.75.2) as	
	donor and ACE2 as acceptor.	
11.19.	Binding free energies (kcal/mol) and its components of S protein	440
	(B.A.2.75)-ACE2 complex obtained using MM-GBSA approach.	
11.20.	Binding free energies (kcal/mol) and its components of S protein	440
	(B.A.2.75.2)-ACE2 complex obtained using MM-GBSA approach.	
Table	Chapter 12	Page
Table No.	Chapter 12	Page No.
	Chapter 12	Ŭ
	Chapter 12 Hydrogen bond analysis of S protein-L-SIGN complex during the last	Ŭ
No.		No.
No.	Hydrogen bond analysis of S protein-L-SIGN complex during the last	No.
No.	Hydrogen bond analysis of S protein-L-SIGN complex during the last 20 ns of MD simulation with S protein as acceptor and L-SIGN as	No.
No.	Hydrogen bond analysis of S protein-L-SIGN complex during the last 20 ns of MD simulation with S protein as acceptor and L-SIGN as donor.	No. 461
No. 12.1. 12.2.	Hydrogen bond analysis of S protein-L-SIGN complex during the last 20 ns of MD simulation with S protein as acceptor and L-SIGN as donor. Hydrogen bond analysis of S protein-L-SIGN complex during the last	No. 461
No.	Hydrogen bond analysis of S protein-L-SIGN complex during the last 20 ns of MD simulation with S protein as acceptor and L-SIGN as donor. Hydrogen bond analysis of S protein-L-SIGN complex during the last 20 ns of MD simulation with S protein as donor and L-SIGN as acceptor. Hydrogen bond analysis of S protein-CAT complex during the last 20	No. 461
No. 12.1. 12.2.	Hydrogen bond analysis of S protein-L-SIGN complex during the last 20 ns of MD simulation with S protein as acceptor and L-SIGN as donor. Hydrogen bond analysis of S protein-L-SIGN complex during the last 20 ns of MD simulation with S protein as donor and L-SIGN as acceptor.	No. 461
No. 12.1. 12.2.	Hydrogen bond analysis of S protein-L-SIGN complex during the last 20 ns of MD simulation with S protein as acceptor and L-SIGN as donor. Hydrogen bond analysis of S protein-L-SIGN complex during the last 20 ns of MD simulation with S protein as donor and L-SIGN as acceptor. Hydrogen bond analysis of S protein-CAT complex during the last 20	No. 461

12.5.	Protein-Protein interface interaction statistics for the S protein-L-SIGN and S protein-CAT complexes obtained from PDBsum server	471
12.6.	List of atom-atom interactions (Hydrogen bonds) across protein-ligand interface in Spike Protein (Chain A) and L-SIGN receptor (Chain B) complex from PDBsum server	472
12.7.	List of atom-atom interactions (non-bonded contacts) across protein- ligand interface in Spike Protein (Chain A) and L-SIGN receptor (Chain B) complex from PDBsum server	473
12.8.	List of atom-atom interactions (Salt bridges) across protein-ligand interface in Spike Protein (Chain A) and L-SIGN receptor (Chain B) complex from PDBsum server	475
12.9.	List of atom-atom interactions (Hydrogen bonds) across protein-ligand interface in Spike Protein (Chain A) and CAT receptor (Chain B) complex from PDBsum server	475
12.10.	List of atom-atom interactions (non-bonded contacts) across protein-ligand interface in Spike Protein (Chain A) and CAT receptor (Chain B) complex from PDBsum server.	476
12.11.	List of atom-atom interactions (Salt bridges) across protein-ligand interface in Spike Protein (Chain A) and CAT receptor (Chain B) complex from PDBsum server.	482
12.12.	Binding free energies (kcal/mol) and its derived components of S protein-L-SIGN and S protein-CAT complexes obtained using HawkDock server.	482

List of Abbreviations

Å	Angstrom
ACE2	Angiotensin Converting Enzyme 2
ARJ	Arjunglucoside-I
AKA	Alpha-ketoamide
AMBER	Assisted Model Building with Energy Refinement
ADMET	Absorption, Distribution, Metabolism, Excretion, and Toxicity
BFE	Binding Free Energy
3CLpro	3-chymotrypsin-like proteases
COVID-19	Coronavirus disease 2019
CTD	C-Terminal Domain
CAN	Carnosol
CASTp	Computed Atlas of Surface Topography of proteins
CoM	Center of Mass
CG	Conjugate Gradient
DM	Double Mutant
DP	Delta-Plus
E protein	Envelope protein
ELE	Electrostatic
EUAs	Emergency Use Authorizations
FAO	Food and Agriculture Organization
FF	Force Field
FFT	Fast Fourier Transform
fs	Femtosecond
FF99SB	Force-field 99 Stony Brook
GI	Gastrointestinal
GBSA	Generalized Born Surface Area
GOR	Garnier-Osguthorpe-Robson
GRAVY	Grand Average of Hydropathicity
g/cc	grams per cubic centimeter
HDAC2	Histone Deacetylase
INSACOG	Indian SARS-CoV-2 Genomics Consortium
kcal/mol	kilocalories per mole
K	kelvin
MW	Molecular Weight
MERS-CoV	Middle East respiratory syndrome
M protein	Membrane protein
Mpro	Main Protease
MHA	Ministry of Home Affairs
MD	Molecular Dynamics
MM	Molecular Mechanics
NDMA	National Disaster Management Authority

List of Abbreviations

NMPA	National Medical Products Administration
N protein	Nucleocapsid protein
NTD	N-Terminal Domain
NHC	National Health Commission
NIH	National Institutes of Health
nsps	nonstructural proteins
ns	nanosecond
nmode	normal mode
NCBI	National Center for Biotechnology Information
nHA	number of hydrogen bond acceptors
nHD	number of hydrogen bond donors
NVT	Nanosecond constant volume
ORFs	Open Reading Frames
PMF	Potential of Mean Force
PRODIGY	PROtein binDIng enerGY prediction
PPIs	Protein-protein interactions
PDB	Protein Data Bank
PLpro	papain-like protease
PONDR	Predictor of naturally disordered regions
PBSA	Poisson-Boltzmann Surface Area
PME	Particle Mesh Ewald
ps	picosecond
pI	Isoelectric point
RT-PCR	Real-Time Reverse-Transcription-Polymerase-Chain-Reaction
RdRp	RNA-dependent RNA-polymerase
RBD	Receptor Binding Domain
RBM	Receptor Binding Motif
RMSD	Root Mean Square Deviation
RMSF	Root Mean Square Fluctuation
RCSB-PDB	Research Collaboratory for Structural Bioinformatics Protein
	Data Bank
ROS	Rosmanol
RCs	Reaction Coordinates
Rg	Radius of Gyration
SARS-CoV-2	Severe Acute Respiratory Syndrome Coronavirus 2
S protein	Spike Protein
SASA	Solvent-Accessible Surface Area
SD	Steepest Descents
TMPRSS2	Transmembrane Serine Protease-2
TM Domain	Transmembrane Domain
TIP3P	Transferable Intermolecular Potential Three-Point
US	Umbrella Sampling

List of Abbreviations

UCSF	University of California, San Francisco
VOC	Variant of Concern
VUI	Variant Under Investigation
VOI	variant of interest
VMD	Visual molecular dynamics
VDW	van der Waals
WHAM	Weighted Histogram Analysis Method
WOAH	World Organization for Animal Health
WHO	World Health Organization
WT	Wild Type
WHAM	Weighted Histogram Analysis Method

List of Publications

This thesis is partly based on the following original communications:

- Das, C., Das, D., and Mattaparthi, V.S.K. Effect of Mutations in the SARS-CoV-2 Spike RBD Region of Delta and Delta-Plus Variants on its Interaction with ACE2 Receptor Protein. *Letters in Applied NanoBioScience*, 12, 118, 2023. DOI: https://doi.org/10.33263/LIANBS124.118
- Das, C., Hazarika, P.J., Deb, A., Joshi, P., Das, D., and Mattaparthi, V.S.K. Effect of Double Mutation (L452R and E484Q) in RBD of Spike Protein on its Interaction with ACE2 Receptor Protein. *Biointerface Research in Applied Chemistry*, 13, 97, 2022. DOI: https://doi.org/10.33263/BRIAC131.097
- 3. **Das, C.**, Das, D., and Mattaparthi, V. S. K. Computational Investigation on the Efficiency of Small Molecule Inhibitors Identified from Indian Spices against SARS-CoV-2 Mpro. *Biointerface Research in Applied Chemistry*, 13(3), 235, 2023. DOI: https://doi.org/10.33263/BRIAC133.235
- 4. **Das, C.**, and Mattaparthi, V. S. K. Impact of Mutations in the SARS-CoV-2 Spike RBD Region of BA.1 and BA.2 Variants on its Interaction with ACE2 Receptor Protein. *Biointerface Research in Applied Chemistry*, 13(4), 358, 2023. DOI: https://doi.org/10.33263/BRIAC134.358
- 5. **Das, C.**, and Mattaparthi, V.S.K. Efficiency of CAT and L-SIGN as Alternative or Coreceptors for SARS-CoV-2 Spike Protein. *Coronaviruses*, 4 (3), 2023. DOI: https://dx.doi.org/10.2174/0126667975262159230927074645
- Das, C., and Mattaparthi, V.S.K. Computational investigation on the Physio-chemical, Structural and Binding features of BA.2.75 and BA.2.75.2 Omicron variants of SARS-CoV-2. Letters in Applied NanoBioScience, 13(4), 191, 2024. DOI: https://doi.org/10.33263/LIANBS134.191
- 7. **Das, C.**, Mohta, A., and Mattaparthi, V.S.K. Computational investigation on the impact of mutations in the SARS-CoV-2 spike RBD region of BA.2.12.1 and BA.4 variants on its interaction with ACE2 Receptor Protein. *Letters in Applied NanoBioScience*, 13, 2, 2024. DOI: https://doi.org/10.33263/LIANBS132.096
- 8. **Das, C.**, and Mattaparthi, V.S.K. Computational Design of Peptide Inhibitors Targeting the SARS-CoV-2 Main Protease. *Coronaviruses*, 5, e130624230993, 2024. DOI: https://doi.org/10.2174/0126667975319992240612053235

Conference Proceedings

- 1. **Das, C.,** and Mattaparthi, V. S. K. "Effect of Double Mutation (L452R and E484Q) in RBD of Spike Protein on its Interaction with ACE2 Receptor Protein" in the *National Seminar on Advances in Basic and Translational Research in Biology (ABTRiB)* organised by department of Molecular Biology and Biotechnology, Tezpur University on 11-12th March 2022. (Poster Presentation)
- 2. **Das, C.,** and Mattaparthi, V. S. K. "Effect of Mutations on the RBD of Spike Protein on its Interaction with ACE2 Receptor Protein of human host" in the 12th India-Japan Science and Technology Conclave: International Conference on Frontier Areas of Science and Technology (ICFAST-2022) held at University of Hyderabad on September 9-10, 2022. (Poster Presentation)
- 3. **Das, C.,** and Mattaparthi, V. S. K. Participated in the "*National-level mentoring symposium "Gurukul in emerging areas in modern biology and medicine*" organized by Indian National Young Academy of Sciences (INYAS) in collaboration with Dept. of Molecular Biology and Biotechnology, Tezpur University on 2nd & 3rd March, 2023. (Participation)
- 4. **Das, C.,** and Mattaparthi, V. S. K. "Efficacy of Alternative receptors (CAT and L-SIGN) for SARS-CoV-2 entry: An in-silico study" on the *National seminar on Research at the Interface of Chemical, Biological and Material Sciences* organized by the Dept. of Chemical sciences in collaboration with Students Science Council on March 10, 2023. (Oral presentation)
- 5. **Das, C.,** and Mattaparthi, V. S. K. Participated in the "demonstration-cum-hands on session on 'AI and DL in Life Science and Healthcare Research" organized by the department of Molecular Biology and Biotechnology, Tezpur University on 10th February 2023. (Participation)
- 6. **Das, C.,** and Mattaparthi, V. S. K. "Computational Investigation on the Efficiency of Small Molecules Identified from Indian Spices acting as inhibitor against SARS-CoV-2 Mpro" in the *TU Science Graduate Research Conclave 2025* organised by the School of Sciences, Tezpur University on 10-11th of February 2025. (Poster Presentation)